Postgrowth Tuning of the Bandgap of Single-Layer Molybdenum Disulfide Films by Sulfur/Selenium Exchange

Quan Ma,[†] Miguel Isarraraz,[†] Chen S. Wang,[†] Edwin Preciado,[†] Velveth Klee,[†] Sarah Bobek,[†] Koichi Yamaguchi,[†] Emily Li,[†] Patrick Michael Odenthal,[†] Ariana Nguyen,[†] David Barroso,[†] Dezheng Sun,[†,§] Gretel von Son Palacio,[†] Michael Gomez,[†] Andrew Nguyen,[†] Duy Le,[‡] Greg Pawin,[†] John Mann,[†] Tony. F. Heinz,[§] Talat Shahnaz Rahman,[‡] and Ludwig Bartels[†,*]

[†]Chemistry, Physics, Electrical Engineering and Materials Science and Engineering, University of California, Riverside, California 92521, United States, [‡]Department of Physics, University of Central Florida, Orlando, Florida 32816, United States, and [§]Departments of Physics and Electrical Engineering, Columbia University, New York, New York 10027, United States

ABSTRACT We demonstrate bandgap tuning of a single-layer MoS_2 film on SiO_2/Si *via* substitution of its sulfur atoms by selenium through a process of gentle sputtering, exposure to a selenium precursor, and annealing. We characterize the substitution process both for S/S and S/Se replacement. Photoluminescence and, in the latter case, X-ray photoelectron spectroscopy provide direct evidence of optical band gap shift and selenium incorporation, respectively. We discuss our experimental observations, including the limit of the achievable bandgap shift, in terms of the role of stress in the film as elucidated by computational studies, based on density functional theory. The resultant films are stable in vacuum, but deteriorate under optical excitation in air.

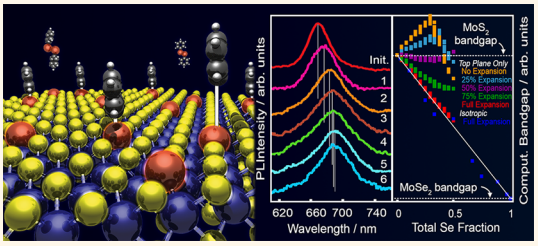

KEYWORDS: molybdenum disulfide · molybdenum diselenide · transition metal dichalcogenides · CVD · sputtering · bandgap engineering · atomically thin films

The development of electronic, photonic, and spintronic devices based on two-dimensional (2D) materials is one of the drivers behind the tremendous interest that materials such as graphene, single-layer MoS_2, and h-BN have attracted over the past years.[1−4] These materials as a group offer high carrier mobility,[5,6] excellent spin transport,[7] direct bandgap semiconducting properties,[2,3,8−11] and valleytronic potential,[8−11] to name a few characteristics. A major opportunity for 2D materials and their applications lies in the tunability of bandgaps and the preparation of heterojunctions from materials with different gaps.[12−14] Recent studies have shown the possibility of tuning the band gap of transition metal dichalcogenides (TMDs) by growing alloys of different Mo/W and S/Se ratios: $Mo_xW_{(1-x)}S_2$, $Mo_xW_{(1-x)}Se_2$, and $MoS_{2(1-x)}Se_{2x}$.[15−21] Complementary to this approach, here we demonstrate the *postgrowth* manipulation of the bandgap of single-layer MoS_2 by means of a simple sputtering-based procedure.

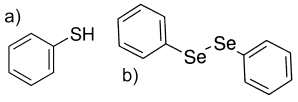

Scheme 1. (a) Benzenethiol (BT); (b) diselenodiphenyl (DS).

Single-layer $MoS_{2(1-x)}Se_{2x}$ alloy films have been grown that exhibit bandgaps that can be tuned continuously between the limits of MoS_2 and $MoSe_2$ (1.87 and 1.55 eV, respectively), as previously predicted theoretically.[22,23] While such large-scale growth of alloys is desirable for certain applications,[24] a method that can alter the bandgap after growth provides other advantages. Here we show the ability to tune the bandgap of single-layer MoS_2 films by means of a sequence of gentle Ar^+-sputtering for removal of top-layer S atoms to yield S vacancies in the film,[25] followed by exposure to an organic selenium source. Subsequent annealing of the film to temperatures as low as 600 K cleaves off the organic moieties, resulting in a film with Se

* Address correspondence to Ludwig.Bartels@ucr.edu.

Received for review January 21, 2014 and accepted March 31, 2014.

Published online March 31, 2014
10.1021/nn5004327

atoms inserted into the S vacancy sites, with a concomitant restoration of the photoluminescence yield. The low process temperature, far below the ~1000 K needed for original film growth, is attractive for device fabrication processes with a limited thermal budget.

Transition metal dichalcogenide single-layer films are composed of a hexagonal Mo-plane, surrounded above and below by planes of chalcogen atoms in displaced hexagonal sites. In this paper, we first characterize the substitution process by examining the removal and subsequent reinsertion of sulfur atoms. We find only a modest net decrease of the photoluminescence efficiency of the material, which is often used as an indicator of its quality.[26−28] We then present results for the insertion of selenium atoms after sputtering by use of a different organic precursor. This procedure is found to reach an apparent limit when approximately half of the top-plane sulfur atoms are replaced by selenium atoms.

We utilize MoS_2 single-layer films that are grown in a CVD method on 300 nm SiO_2/Si substrates, which we have previously described.[19,29] All measurements proceed in an ultrahigh vacuum (UHV) apparatus that permits *in vacuo* sputtering, X-ray photoelectron spectroscopy (XPS), and photoluminescence (PL) measurements.

Removal of sulfur atoms proceeds *via* exposure of the sample to a 500 V Ar^+-beam, as described in literature.[25] Immediately following sulfur removal, we expose the sample to 3 L of either benzenethiol (BT) or diselenodiphenyl (DS) (Scheme 1, both from Aldrich) through a leak valve and through evaporation from a glass capillary, respectively. We then anneal the sample to ~600 K by means of indirect heating for 10 min. The temperature is measured on the sample holder. We perform PL and XPS measurements after cool-down to room temperature. More experimental details can be found in the Methods section.

RESULTS

Before discussing insertion of Se into a single-layer MoS_2 film, we characterize the method for the reinsertion of sulfur atoms. Figure 1a shows the PL intensity of an as-prepared (red) single-layer MoS_2 film as a function of temperature, revealing a well-studied decrease in PL yield with increasing temperature.[27,30−32] Adsorption of 3 L of BT, an organic sulfur source, at 150 K reduces the MoS_2 PL yield. Upon heating the sample above ~180 K, BT is desorbed intact, as verified by mass spectrometry. We find that strength and the spectral position of the PL then return to the values found for bare MoS_2 (Figure 1a and inset). The recovery of the PL properties of the MoS_2 single-layer film after BT desorption indicates the inertness and stability of the MoS_2 film (prior to activation by sputtering) to exposure to the chalcogen source.

Activation of the MoS_2 film through sputtering reduces its PL yield significantly as a consequence of

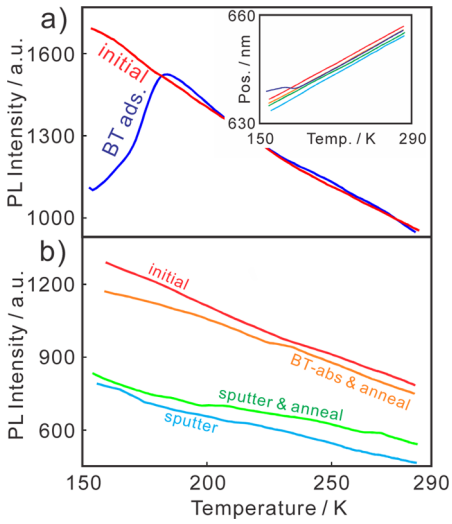

Figure 1. (a) PL intensity of an as-prepared (red) MoS_2 film and after 3 L BT-exposure at 150 K as a function of substrate temperature. Upon BT desorption at ~180 K (as verified by mass spectrometry), the PL intensity and PL position (inset) recover their original values. (b) PL of the MoS_2 single-layer film prior to (red) and after (blue) sputtering. Data are also shown after a subsequent annealing to 600 K (green), followed by BT absorption and a further annealing cycle (orange). The PL intensity and spectral position (inset) essentially recover their original values.

increased nonradiative exciton recombination at defect sites.[25] This behavior is apparent by comparison of the red and blue lines in Figure 1b. Annealing the film to 600 K (green line) results in partial recovery of the PL yield, presumably through local healing of film defects. Subsequent exposure of the activated film to BT at room temperature, followed by annealing to 600 K, restores the room-temperature PL intensity. We attribute this to the film extracting sulfur from the BT precursor through a process analogous to the use of MoS_2 as a hydrodesulfurization catalyst.[33] We note that in prior measurements on metal surfaces we found S−C bond scission at comparable and even lower temperatures.[34,35]

While the recovery at room temperature very nearly reaches the original level, at lower temperatures a modest reduction in the overall PL yield is still present. We attribute this to longer exciton lifetimes at low temperatures allowing the excitons to diffuse more readily to defect sites for nonradiative recombination.[31] This effect can be reduced further by avoiding the annealing step (green line) between sputtering of the film and the chalcogen exposure. We anticipate that optimization of the process parameters (amount of sulfur removed per cycle, BT exposure, annealing temperature, *etc.*) will further improve the film quality. The sputtered films show a slight blue shift of the PL spectrum (see inset of Figure 1), which disappears after sulfur reinsertion.

If we use DS (the organic selenium precursor) instead of BT, the behavior is fundamentally different:

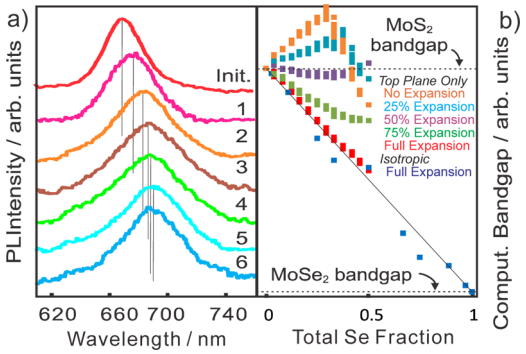

Figure 2. (a) Normalized room-temperature PL spectra of a single-layer MoS_2 film after sputtering and DS insertion cycles. The PL peak red shifts and broadens until saturation is reached. The vertical lines indicate the peak position as a guide to the eye. (b) DFT-based bandgap of $MoS_{2(1-x)}Se_{2x}$ between the limits of pure MoS_2 and pure $MoSe_2$ for homogeneous $MoS_{2(1-x)}Se_{2x}$ (blue, from ref 19) and for insertion of Se exclusively into the top chalcogen plane (red). Insertion of Se causes lateral expansion of the film lattice ($MoSe_2$ has a lattice constant ~4% larger than MoS_2). Restriction of lattice expansion to a certain percentage of the equilibrium value for any Se concentration results in the bandgap values shown in green, pale blue, purple, and brown. The height of the data points indicates the spread of values for different arrangements of the Se atoms in the computational supercell. Because the levels of theory used in ref 19 and in the present work underestimate TMD bandgaps to different degrees, the values are indicated with respect to the bandgaps calculated for the pure (MoS_2 or $MoSe_2$) and relaxed TMDs found in each approach.

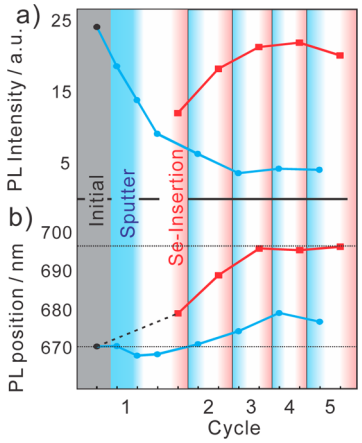

Figure 3. Room-temperature PL intensities and peak positions of a MoS_2 single-layer film after cycles of sputtering and DS exposure. (Top) Repeated sputtering reduces the initial PL intensity (blue). When DS insertion steps are interspersed with sputtering cycles, the film's PL yield nearly recovers to its initial value. (Bottom) Sputtering blue-shifts the PL peak position; insertion of Se causes a red shift that saturates after approximately the third insertion cycle. The peak position shifts by a total of 27 nm or 71 meV.

while we still observe significant recovery of the PL yield after exposure and annealing, the spectral position of the PL shifts to longer wavelengths, as expected for the insertion of Se into the film. Figure 2 shows PL spectra acquired on a single-layer MoS_2 film as a function of the number of DS insertion cycles. Initially, we find the typical emission of MoS_2 at 670 nm. With increasing number of insertion cycles, the PL feature shifts continuously to longer wavelengths. The PL emission spectrum remains a single, well-defined peak, consistent with recent findings for $MoS_{2(1-x)}Se_{2x}$ single-layer alloy films and indicating the formation of a relatively homogeneous film.

Figure 3 summarizes an experiment in which we highlight the ability to recover the PL intensity by reinsertion of Se atoms. We first treat the sample by sputtering for three cycles, each sputtering process reducing the film's PL yield (Figure 3a, blue line). On the basis of the data of ref 25, this suggests the removal of almost 10% of the sulfur atoms. Exposure to DS after the third cycle partially restores the film's PL yield (red line). Subsequent cycles of sputtering and DS insertion further increase the PL to approximately 90% of the original intensity. We attribute the residual decrease in PL to a combination of a slightly lower PL yield in $MoS_{2(1-x)}Se_{2x}$ as compared to MoS_2 and sputter damage that is not completely healed during the Se insertion cycles. If we perform only a single sputter cycle prior to the first selenium insertion step, as was done for the measurements presented in Figures 2 and 4, this effect is less pronounced.

The spectral shift of the PL decreases in successive cycles of sputtering and Se insertion. This behavior can be rationalized by the decreasing fraction of S atoms exposed in the MoS_2 film in successive cycles; we discuss this effect below in detail. The final PL spectral shift varies in the range between 20 and 30 nm from sample to sample. The terminal red shift of the sample of Figure 3 of 27 nm corresponds to a bandgap shift of 0.07 eV, almost one-quarter of the difference between the MoS_2 and $MoSe_2$ bandgaps. Previous experimental work on $MoS_{2(1-x)}Se_{2x}$ films revealed a nearly linear dependence of the PL emission energy on Se content.[19] On the basis of that work, the PL shift corresponds to replacement of 21% of the total sulfur content of MoS_2 by selenium atoms. Once this point is reached, subsequent sputter-insertion cycles do not appreciably shift the PL position, but induce a slight deterioration of the overall PL yield, presumably reflecting sputter defects that are not fully annealed.

We use XPS to confirm the insertion of selenium into our films after the modification process. Figure 4 shows a sequence of spectra of the relevant core-level peaks for the sample of Figure 2. With the exception of the rise of the Se 3d peak and reduction of the S 2p peaks (by ~22%), we do not observe a change in the sample's features. We also monitored the area of the carbon 1s peak, but did not find a significant signature of this element (see Supporting Information). While the XPS results indicate S/Se exchange consistent with the shift of the optical bandgap, these measurements may be affected by systematic errors associated with removal of excess sulfur from or attachment of excess selenium to the film or the substrate surface.

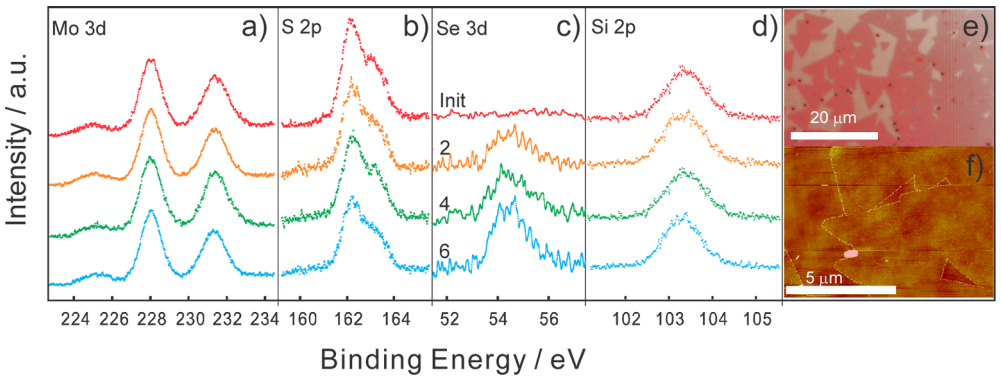

Figure 4. XPS spectra of the sample of Figure 2 after 0, 2, 4, 6 cycles of selenium insertion. (a–d) Mo 3d, S 2p, Se 3d, and Si 2p substrate peaks, respectively. Initially no selenium is signature is found. Its presence is visible after 2 cycles and increases with the number of cycles, with a concomitant decrease in the sulfur signal. (e and f) Optical and AFM microscopy in air of the edge of the MoS_2 film after 6 selenium insertion cycles. The flat and smooth triangular islands and regions of continuous film are indistinguishable from images of the untreated film.

We performed *ex situ* optical and AFM imaging of the film after Se insertion and found it to be as flat and as smooth as before the treatment (Figure 4e,f). Analysis of height traces on the MoS_2 film prior and after S/Se exchange shows roughness of 0.45 and 0.05 nm over 5 μm, practically unchanged values that primarily reflect the resolution of the instrument and flatness of the underlayer, and rule out significant rearrangement of the film material.

Our previous study shows that the mild sputtering process does not remove an appreciable amount of Mo from the film and that the XPS Mo electronic configuration remains unchanged,[25] suggesting the overall structural stability of the chalcogen-depleted film in vacuum. In air, however, the sputtered films deteriorate. *Ex situ* PL measurements in air of the samples after Se insertion using a Raman microscope (Horiba LabRam) show rapid sample deterioration during optical excitation. We attribute this degradation to the presence of a comparatively low density of unsaturated bonds/sites from sputter damage to the film. Future work will address avenues for film passivation through *in situ* capping by a barrier layer.

DISCUSSION

Having demonstrated the insertion of Se into our films, we turn to the observation of a terminal bandgap that falls short of the optical bandgap shift expected for complete S/Se exchange. Insertion of Se from an organic source at comparatively low annealing temperature may favor insertion into the top chalcogen plane.[19,23] We performed density functional theory (DFT) calculations to determine the expected behavior in the limiting case of insertion of Se exclusively into the top chalcogen plane (the Supporting Information provides computational details). We utilize 6×6 MoX_2 supercells and compute bandgaps for different top-plane arrangements of Se and S atoms. Figure 2b compares the bandgap predictions for homogeneous $MoS_{2(1-x)}Se_{2x}$ single-layer alloy films (blue, from ref 19 similar to results in ref 23) with the behavior expected for strictly top-layer insertion (red). The bandgap for the same Se content are seen to be quite similar.

We note, however, that insertion of Se induces expansion of the equilibrium $MoS_{2(1-x)}Se_{2x}$ lattice constant. The computed equilibrium lattice spacings for top-plane and homogeneous Se insertion do not differ meaningfully for the same total Se content and suggest a 4% increase for $MoSe_2$ compared with MoS_2, in line with literature values.[22,23] The degree of expansion of the treated films is not known directly from experiment. The nucleation sites for film growth[36,37] may serve as pinning centers for the film, preventing complete lateral expansion, especially for the case of the continuous films as used in this work.[29] We have accordingly analyzed the film's bandgap for different fractions of the equilibrium expansion for various Se concentrations (top four traces in Figure 2b). In the absence of an expansion (brown trace), the competition between Se insertion (leading to decreased bandgap)[22,23] and compressive strain of the film (leading to increased bandgap with small compressive strain)[38,39] causes the bandgap to deviate significantly from the case in which strain is relaxed. For low Se concentrations, the gap widens slightly, followed by narrowing at higher Se concentrations. For partial lattice relaxation, the variation of the bandgap with the Se contents becomes smaller, and at 50% relaxation, the initial bandgap widening vanishes, in good agreement with our experimental results. However, even at 75% of the equilibrium expansion, we still find a marked distinction from the equilibrium case, leading to a bandgap reduction for complete S/Se exchange in the top layer that is compatible with our experimentally observed value. We conclude that partial pinning of the film on the substrate, and the associated lack of lattice relaxation, may reduce the variation of the bandgap with Se-content. This suggests that the observed reduction in bandgap shift with increased cycle number (Figure 2a) may also reflect an increase in

strain in the film, rather than exclusively a reduction of the amount of inserted Se.

Thus, although both XPS and the PL suggest some 22% exchange of S by Se, the precise match of these values may reflect possible systematic error in XPS and underestimation of the Se-insertion from the PL measurements of the bandgap. We note that our computational approach with periodic supercells does not allow for bending of the film as a consequence of Se insertion. We have performed calculations of phonon dispersions (see Supporting Information) and find dynamic stability of the flat, free-standing film at any top-layer Se concentration. We note, however, that a combination of a bending in the film and pinning to the substrate may generate a limit to stable Se insertion short of complete S/Se exchange. These issues will be examined in future measurements starting from Se-rich material.

CONCLUSION

The simple procedure presented here to tune the bandgap of single-layer transition metal dichalcogenide films after growth suggests new research directions. Local spatial patterning of the bandgap should be possible by control of the sputtered region of the film. This would provide a means to produce heterojunctions and spatial variation of the bandgap for other purposes. At the same time, this study shows that induced strain in the film may play an important role, providing another route for control of the bandgap.

METHODS

Initial film growth was achieved in a tube furnace at ~1000 K using SiO_2/Si substrates of ~2 cm × 2 cm in size. MoO_3 powder and liquid BT were used as metal and chalcogen sources, respectively. Our setup and method are described in detail in previous publications.[19,29]

All experiments were carried out in an ultrahigh vacuum (UHV) chamber with a base pressure of 5×10^{-10} Torr. This system is equipped with an ion sputter gun (Varian), an hemispherical electron energy analyzer (Scientia VG R3000), and a Mg X-ray source for X-ray photoelectron spectroscopy (XPS). The XPS analyzer collects electrons from a 0.6 mm × 4 mm area on the sample.

The apparatus permits PL spectroscopy from the sample within the UHV chamber. This is accomplished using an external 532 nm solid-state laser for excitation, a 50 mm lens within the chamber for focusing and collecting the photoluminescence, and a spectrometer (Verity SD 1024) with a cooled CCD array for PL detection. The laser power on the sample was ~20 mW, focused to a spot diameter of ~100 μm.

Each sputter cycle takes 4 ± 1 s and is performed with the sample held at room temperature. We use a beam current of 0.6 μA, with a separation between ion gun and sample of ~16 cm. We anneal the sample to ~600 K by means of indirect heating for 10 min. The temperature is measured on the sample holder. We perform PL and XPS measurements after cool-down.

AFM measurements utilize a Dimension 3100 Nanoman by Veeco using silicon coated tips by Bruker. AFM images reveal features of angstrom-scale height on the SiO_2 substrate, but the MoS_2 films appear smooth both before and after the procedure described in this manuscript. Calculations were performed using density functional theory, details of which can be found in the Supporting Information section.

Conflict of Interest: The authors declare no competing financial interest.

Acknowledgment. L.B. gratefully acknowledges support by C-SPIN, one of six centers supported by the STARnet phase of the Focus Center Research Program (FCRP), a Semiconductor Research Corporation program sponsored by MARCO and DARPA. Work of the Bartels and Heinz groups on the film growth was supported by the U.S. National Science Foundation under Grants DMR-1106210 and DMR-1106172, respectively. XPS analysis and theoretical modeling of the films were made possible by a grant by the U.S. Department of Energy (UCR, UCF, Columbia University: DE-FG02-07ER15842). Computational collaboration between L.B.'s and T.S.R's group is supported by resources provided by NERSC (DE-AC02-05CH11231) and the Extreme Science and Engineering Discovery Environment (project TG-DMR130009), respectively. M.I. and C.S.W. were supported by NSF graduate fellowships DGE-1326120. We thank R. Kawakami of Ohio State University for helpful discussions.

Supporting Information Available: Electronic structure, vibronic structure, and phonon dispersions calculations for $MoS_{2-x}Se_x$ structures, XPS characterizations of the carbon 1s peak in selenized MoS_2 samples. This material is available free of charge *via* the Internet at http://pubs.acs.org.

REFERENCES AND NOTES

1. Geim, A. K.; Novoselov, K. S. The Rise of Graphene. *Nat. Mater.* **2007**, *6*, 183–191.
2. Mak, K. F.; Lee, C.; Hone, J.; Shan, J.; Heinz, T. F. Atomically Thin MoS_2: A New Direct-Gap Semiconductor. *Phys. Rev. Lett.* **2010**, *105*, 136805.
3. Splendiani, A.; Sun, L.; Zhang, Y.; Li, T.; Kim, J.; Chim, C. Y.; Galli, G.; Wang, F. Emerging Photoluminescence in Monolayer MoS_2. *Nano Lett.* **2010**, *10*, 1271–1275.
4. Dean, C.; Young, A.; Meric, I.; Lee, C.; Wang, L.; Sorgenfrei, S.; Watanabe, K.; Taniguchi, T.; Kim, P.; Shepard, K. Boron Nitride Substrates for High-Quality Graphene Electronics. *Nat. Nanotechnol.* **2010**, *5*, 722–726.
5. Zhang, Y.; Tan, Y. W.; Stormer, H. L.; Kim, P. Experimental Observation of the Quantum Hall Effect and Berry's Phase in Graphene. *Nature* **2005**, *438*, 201–204.
6. Radisavljevic, B.; Radenovic, A.; Brivio, J.; Giacometti, V.; Kis, A. Single-Layer MoS_2 Transistors. *Nat. Nanotechnol.* **2011**, *6*, 147–150.
7. Kane, C.; Mele, E. Quantum Spin Hall Effect in Graphene. *Phys. Rev. Lett.* **2005**, *95*, 226801.
8. Cao, T.; Wang, G.; Han, W.; Ye, H.; Zhu, C.; Shi, J.; Niu, Q.; Tan, P.; Wang, E.; Liu, B.; *et al.* Valley-Selective Circular Dichroism of Monolayer Molybdenum Disulphide. *Nat. Commun.* **2012**, *3*, No. 887.
9. Mak, K. F.; He, K.; Shan, J.; Heinz, T. F. Control of Valley Polarization in Monolayer MoS_2 by Optical Helicity. *Nat. Nanotechnol.* **2012**, *7*, 494–498.
10. Xiao, D.; Liu, G. B.; Feng, W.; Xu, X.; Yao, W. Coupled Spin and Valley Physics in Monolayers of MoS_2 and Other Group-VI Dichalcogenides. *Phys. Rev. Lett.* **2012**, *108*, 196802.
11. Zeng, H.; Dai, J.; Yao, W.; Xiao, D.; Cui, X. Valley Polarization in MoS_2 Monolayers by Optical Pumping. *Nat. Nanotechnol.* **2012**, *7*, 490–493.
12. Butler, S. Z.; Hollen, S. M.; Cao, L.; Cui, Y.; Gupta, J. A.; Gutierrez, H. R.; Heinz, T. F.; Hong, S. S.; Huang, J.; Ismach, A. F.; *et al.* Progress, Challenges, and Opportunities in Two-Dimensional Materials Beyond Graphene. *ACS Nano* **2013**, *7*, 2898–2926.

13. Chhowalla, M.; Shin, H. S.; Eda, G.; Li, L. J.; Loh, K. P.; Zhang, H. The Chemistry of Two-Dimensional Layered Transition Metal Dichalcogenide Nanosheets. *Nat. Chem.* **2013**, *5*, 263–275.
14. Wang, Q. H.; Kalantar-Zadeh, K.; Kis, A.; Coleman, J. N.; Strano, M. S. Electronics and Optoelectronics of Two-Dimensional Transition Metal Dichalcogenides. *Nat. Nanotechnol.* **2012**, *7*, 699–712.
15. Dumcenco, D. O.; Kobayashi, H.; Liu, Z.; Huang, Y. S.; Suenaga, K. Visualization and Quantification of Transition Metal Atomic Mixing in $Mo_{1-x}W_xS_2$ Single Layers. *Nat. Commun.* **2013**, *4*, No. 1351.
16. Chen, Y.; Xi, J.; Dumcenco, D. O.; Liu, Z.; Suenaga, K.; Wang, D.; Shuai, Z.; Huang, Y. S.; Xie, L. Tunable Band Gap Photoluminescence from Atomically Thin Transition-Metal Dichalcogenide Alloys. *ACS Nano* **2013**, *7*, 4610–4616.
17. Chen, Y.; Dumcenco, D. O.; Zhu, Y.; Zhang, X.; Mao, N.; Feng, Q.; Zhang, M.; Zhang, J.; Tan, P. H.; Huang, Y. S.; *et al.* Composition-Dependent Raman Modes of $Mo_{1-x}W_xS_2$ Monolayer Alloys. *Nanoscale* **2014**, *6*, 2833–2839.
18. Tongay, S.; Narang, D. S.; Kang, J.; Fan, W.; Ko, C.; Luce, A. V.; Wang, K. X.; Suh, J.; Patel, K. D.; Pathak, V. M.; *et al.* Two-Dimensional Semiconductor Alloys: Monolayer $Mo_{1-x}W_xSe_2$. *Appl. Phys. Lett.* **2014**, *104*, 012101.
19. Mann, J.; Ma, Q.; Odenthal, P. M.; Isarraraz, M.; Le, D.; Preciado, E.; Barroso, D.; Yamaguchi, K.; Son, G.v.; Nguyen, A.; *et al.* 2-Dimensional Transition Metal Dichalcogenides with Tunable Direct Band Gaps: $MoS_{2(1-X)}Se_{2x}$ Monolayers. *Adv. Mater.* **2013**, *26*, 1399–1404.
20. Li, H.; Duan, X.; Wu, X.; Zhuang, X.; Zhou, H.; Zhang, Q.; Zhu, X.; Hu, W.; Ren, P.; Guo, P.; Ma, L.; Fan, X.; Wang, X.; Xu, J.; Pan, A.; Duan, X. Growth of Alloy $MoS_{2x}Se_{2(1-x)}$ Nanosheets with Fully Tunable Chemical Compositions and Optical Properties. *J. Am. Chem. Soc.* **2014**, *136*, 3756–3759.
21. Gong, Y.; Liu, Z.; Lupini, A. R.; Shi, G.; Lin, J.; Najmaei, S.; Lin, Z.; Elías, A. L.; Berkdemir, A.; You, G.; Terrones, H.; Terrones, M.; Vajtai, R.; Pantelides, S. T.; Pennycook, S. J.; Lou, J.; Zhou, W.; Ajayan, P. M. Band Gap Engineering and Layer-by-Layer Mapping of Selenium-Doped Molybdenum Disulfide. *Nano Lett.* **2013**, *14*, 442–449.
22. Komsa, H. P.; Krasheninnikov, A. V. Two-Dimensional Transition Metal Dichalcogenide Alloys: Stability and Electronic Properties. *J. Phys. Chem. Lett.* **2012**, *3*, 3652–3656.
23. Kang, J.; Tongay, S.; Li, J.; Wu, J. Monolayer Semiconducting Transition Metal Dichalcogenide Alloys: Stability and Band Bowing. *J. Appl. Phys.* **2013**, *113*, 143703.
24. Yu, Y.; Li, C.; Liu, Y.; Su, L.; Zhang, Y.; Cao, L. Controlled Scalable Synthesis of Uniform, High-Quality Monolayer and Few-Layer MoS_2 Films. *Sci. Rep.* **2013**, *3*, 1866.
25. Ma, Q.; Odenthal, P. M.; Mann, J.; Le, D.; Wang, C. S.; Zhu, Y. M.; Chen, T. Y.; Sun, D. Z.; Yamaguchi, K.; Tran, T.; *et al.* Controlled Argon Beam-Induced Desulfurization of Monolayer Molybdenum Disulfide. *J. Phys.: Condens. Matter* **2013**, *25*, 252201.
26. Sercombe, D.; Schwarz, S.; Pozo-Zamudio, O. D.; Liu, F.; Robinson, B. J.; Chekhovich, E. A.; Tartakovskii, I. I.; Kolosov, O.; Tartakovskii, A. I. Optical Investigation of the Natural Electron Doping in Thin MoS_2 Films Deposited on Dielectric Substrates. *Sci. Rep.* **2013**, *3*, 3489.
27. Eda, G.; Yamaguchi, H.; Voiry, D.; Fujita, T.; Chen, M.; Chhowalla, M. Photoluminescence from Chemically Exfoliated MoS_2. *Nano Lett.* **2011**, *11*, 5111–5116.
28. Ji, Q.; Zhang, Y.; Gao, T.; Zhang, Y.; Ma, D.; Liu, M.; Chen, Y.; Qiao, X.; Tan, P.-H.; Kan, M.; *et al.* Epitaxial Monolayer MoS_2 on Mica with Novel Photoluminescence. *Nano Lett.* **2013**, *13*, 3870–3877.
29. Mann, J.; Sun, D.; Ma, Q.; Preciado, E.; Yamaguchi, K.; Chen, J.-R.; Heinz, T. F.; Kawakami, R.; Bartels, L. Facile Growth of Sub-Millimeter Scale Monolayer MoS_2 Films on SiO_2/Si. *Eur. Phys. J. B* **2013**, *86*, No. 226.
30. Plechinger, G.; Schrettenbrunner, F. X.; Eroms, J.; Weiss, D.; Schüller, C.; Korn, T. Low-Temperature Photoluminescence of Oxide-Covered Single-Layer MoS_2. *Phys. Status Solidi RRL* **2012**, *6*, 126–128.
31. Korn, T.; Heydrich, S.; Hirmer, M.; Schmutzler, J.; Schueller, C. Low-Temperature Photocarrier Dynamics in Monolayer MoS_2. *Appl. Phys. Lett.* **2011**, *99*, No. 102109.
32. Tongay, S.; Zhou, J.; Ataca, C.; Lo, K.; Matthews, T. S.; Li, J.; Grossman, J. C.; Wu, J. Thermally Driven Crossover from Indirect toward Direct Bandgap in 2d Semiconductors: $MoSe_2$ *versus* MoS_2. *Nano Lett.* **2012**, *12*, 5576–5580.
33. Besenbacher, F.; Brorson, M.; Clausen, B. S.; Helveg, S.; Hinnemann, B.; Kibsgaard, J.; Lauritsen, J. V.; Moses, P. G.; Nørskov, J. K.; Topsøe, H. Recent Stm, Dft and Haadf-Stem Studies of Sulfide-Based Hydrotreating Catalysts: Insight into Mechanistic, Structural and Particle Size Effects. *Catal. Today* **2008**, *130*, 86–96.
34. Kim, D.; Sun, D. Z.; Lu, W. H.; Cheng, Z. H.; Zhu, Y. M.; Le, D.; Rahman, T. S.; Bartels, L. Toward the Growth of an Aligned Single-Layer MoS_2 Film. *Langmuir* **2011**, *27*, 11650–11653.
35. Wong, K. L.; Lin, X.; Kwon, K. Y.; Pawin, G.; Rao, B. V.; Liu, A.; Bartels, L.; Stolbov, S.; Rahman, T. S. Halogen-Substituted Thiophenol Molecules on Cu(111). *Langmuir* **2004**, *20*, 10928–10934.
36. Lee, Y. H.; Zhang, X. Q.; Zhang, W.; Chang, M. T.; Lin, C. T.; Chang, K. D.; Yu, Y. C.; Wang, J. T. W.; Chang, C. S.; Li, L. J.; *et al.* Synthesis of Large-Area MoS_2 Atomic Layers with Chemical Vapor Deposition. *Adv. Mater.* **2012**, *24*, 2320–2325.
37. Najmaei, S.; Liu, Z.; Zhou, W.; Zou, X.; Shi, G.; Lei, S.; Yakobson, B. I.; Idrobo, J. C.; Ajayan, P. M.; Lou, J. Vapour Phase Growth and Grain Boundary Structure of Molybdenum Disulphide Atomic Layers. *Nat. Mater.* **2013**, *12*, 754–759.
38. Yun, W. S.; Han, S. W.; Hong, S. C.; Kim, I. G.; Lee, J. D. Thickness and Strain Effects on Electronic Structures of Transition Metal Dichalcogenides: 2H-MX_2 Semiconductors (M = Mo, W; X = S, Se, Te). *Phys. Rev. B* **2012**, *85*, No. 033305.
39. Lu, P.; Wu, X. J.; Guo, W. L.; Zeng, X. C. Strain-Dependent Electronic and Magnetic Properties of MoS_2 Monolayer, Bilayer, Nanoribbons and Nanotubes. *Phys. Chem. Chem. Phys.* **2012**, *14*, 13035–13040.